ACCOUNTS
of chemical research

Methods for Describing the Electromagnetic Properties of Silver and Gold Nanoparticles

JING ZHAO, ANATOLIY O. PINCHUK, JEFFREY M. MCMAHON, SHUZHOU LI, LOGAN K. AUSMAN, ARIEL L. ATKINSON, AND GEORGE C. SCHATZ*

Department of Chemistry, Northwestern University, Evanston, Illinois 60208-3113

RECEIVED ON JANUARY 30, 2008

CONSPECTUS

This Account provides an overview of the methods that are currently being used to study the electromagnetics of silver and gold nanoparticles, with an emphasis on the determination of extinction and surface-enhanced Raman scattering (SERS) spectra. These methods have proven to be immensely useful in recent years for interpreting a wide range of nanoscience experiments and providing the capability to describe optical properties of particles up to several hundred nanometers in dimension, including arbitrary particle structures and complex dielectric environments (adsorbed layers of molecules, nearby metal films, and other particles). While some of the methods date back to Mie's celebrated work a century ago, others are still at the forefront of algorithm development in computational electromagnetics.

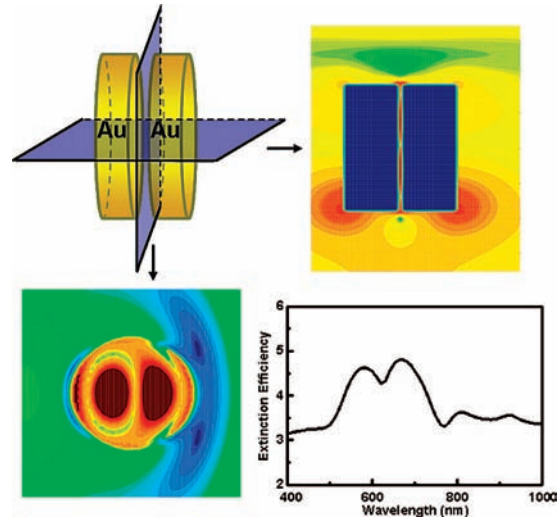

This Account gives a qualitative description of the physical and mathematical basis behind the most commonly used methods, including both analytical and numerical methods, as well as representative results of applications that are relevant to current experiments. The analytical methods that we discuss are either derived from Mie theory for spheres or from the quasistatic (Gans) model as applied to spheres and spheroids. In this discussion, we describe the use of Mie theory to determine electromagnetic contributions to SERS enhancements that include for retarded dipole emission effects, and the use of the quasistatic approximation for spheroidal particles interacting with dye adsorbate layers. The numerical methods include the discrete dipole approximation (DDA), the finite difference time domain (FDTD) method, and the finite element method (FEM) based on Whitney forms. We discuss applications such as using DDA to describe the interaction of two gold disks to define electromagnetic hot spots, FDTD for light interacting with metal wires that go from particle-like plasmonic response to the film-like transmission as wire dimension is varied, and FEM studies of electromagnetic fields near cubic particles.

1. Introduction

Noble metal nanoparticles (or metal films) have been of widespread interest in the past few years as a result of advances in molecular plasmonic devices,[1] biosensing,[2] and other applications. While the most common optical measurements refer to extinction and Rayleigh scattering, there has also been interest in surface-enhanced Raman scattering (SERS) and in a variety of nonlinear optical measurements. Much of this activity is concerned with plasmon resonance excitation in the nanoparticles, in which the electromagnetic field excites collective oscillations of the conduction electrons.[3,4] Such excitations depend strongly on nanoparticle shape, size, and dielectric environment, and as result, they can be tailored for applications at desired wavelengths through particle synthesis. In addition, the plasmon resonance

Published on the Web 08/20/2008 www.pubs.acs.org/acr
10.1021/ar800028j CCC: $40.75

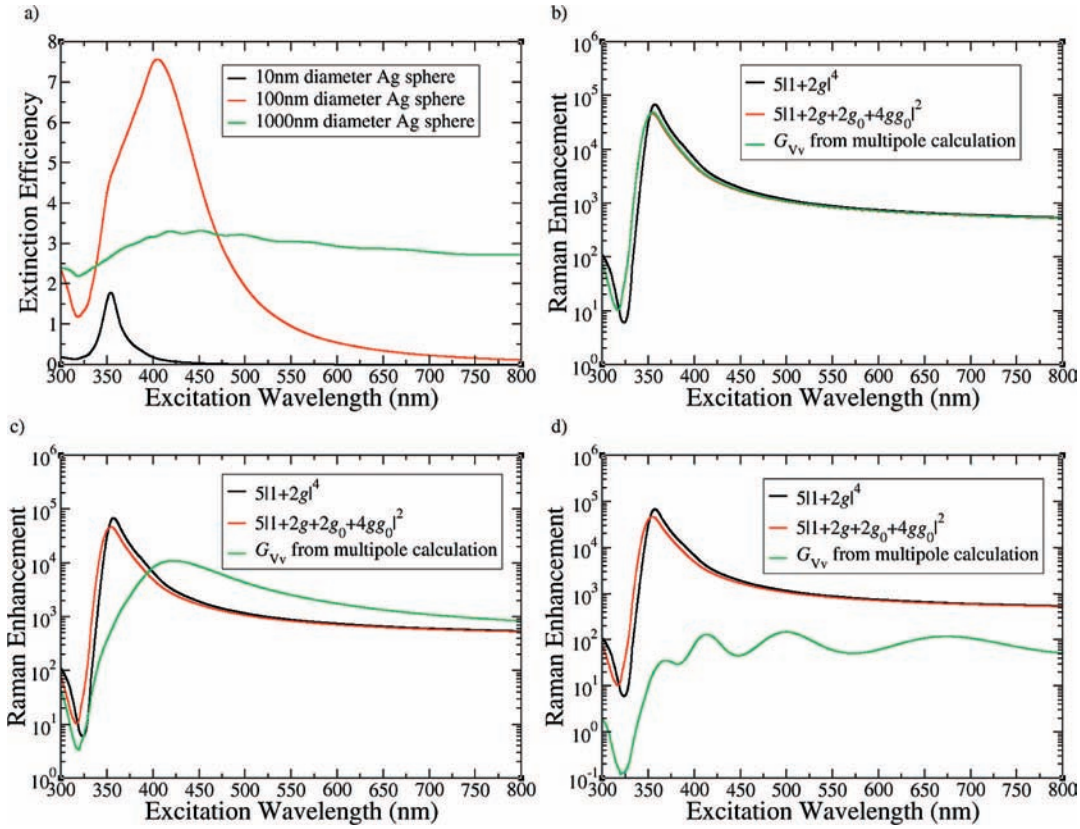

FIGURE 1. Extinction efficiency vs excitation wavelength (a) for Ag spheres with diameters of 10 (black), 100 (red), and 1000 nm (green) and plots of Raman enhancement vs excitation wavelength for 10 (b), 100 (c), and 1000 nm (d). The green lines are the enhancements G_{Vv} calculated using the multipole expansion. The red and black lines are the quasistatic enhancements $5|1 + 2g + 2g_0 + 4gg_0|^2$ and $5|1 + 2g|^4$.

wavelength of a given nanostructure is extremely sensitive to the presence of molecules near the nanostructure, so the shift in this wavelength upon analyte binding can be used in refractive index sensors.[2,5] As a result, a large number of sensing applications have been reported,[5−8] including the study of analytes with molecular resonances in the visible wavelength region.[9,10] In addition, sensing applications using particle aggregation[11] and SERS[2,12] have been reported.

Theory has long played a role in the modeling of metal nanoparticle optical properties, and this role has significantly increased in the last 10 years.[13−19] Almost 100 years ago, it was realized, thanks to the celebrated work of Mie[20] (along with important contributions from many others, as described by Kerker[21]), that classical electromagnetic theory (i.e., solving Maxwell's equations for light interacting with a particle) provides a quantitative description of the extinction and scattering spectra of nanoparticles. Mie's work referred to light scattering from a spherical particle, and thus was not able to describe shape effects, but much of the colloid chemistry work, which dominated the field prior to 1990, involved broad distributions of particle shape and size such that a more quantitative electromagnetic description was not very useful. However the advent of lithographic methods for making nanoparticles has changed the demands on theory for these problems, and as a result there is now interest in describing the optical properties of nonspherical particles, particles in anisotropic dielectric environments, holes in metal films and many other complex nanostructures, such that it is useful to have numerical approaches available for these problems.

This paper provides an overview of the methods that have been developed to describe the optical properties of noble metal nanoparticles, going all the way from Mie theory and other analytical methods, to a variety of numerical methods that can be used to describe complex nanostructures. Although Mie theory is well-known, new applications of it continue to appear, and we will illustrate this through an evaluation of the electromagnetic contribution to SERS enhancements for a molecule interacting with a silver sphere.

Other particle shapes, such as spheroids, also admit to exact solutions, but the solutions are harder to use. One of the most useful alternatives has been the quasistatic approximation, in which Maxwell's equations are replaced by electrostatics (LaPlace equation) but still using frequency-dependent dielectric functions. This Account will describe applications of this approach to the treatment of spheroids interacting with dye molecule adsorbates.

Numerical methods for solving Maxwell's equations come in many different flavors, and our presentation will cover three of the most common methods. The discrete dipole approximation (DDA) is a frequency domain approach that approximates the induced polarization in a complex particle by the response of a cubic grid of polarizable dipoles. The polarizabilities of the dipoles can be chosen so that bulk materials will behave the same as the continuum solution to Maxwell's equations, but the treatment for finite particles is only approximate. However the approximation is accurate enough for many applications, and the computational simplifications afforded by DDA over other methods are such that this method has been very widely used. As an illustration of this, we consider the extinction spectra and electromagnetic hot spots formed from two interacting gold disks, each 120 nm in height and 360 nm in diameter.

One of the simplest of the nominally exact methods is the finite difference time domain (FDTD) method, in which a clever finite differencing algorithm developed by Yee[22] is applied to Maxwell's equations, using grids for the electric field **E** and magnetic field **H**, which are shifted by half a grid spacing relative to each other. This method can be applied in both two and three dimensions, and we provide an example where the 2D algorithm is used to study the transmission of light through a particle array. A third type of numerical approach is the finite element method (FEM), in which the solutions to Maxwell's equations are expanded in locally defined basis functions chosen such that boundary conditions are satisfied on the surfaces of the elements. Here we consider the so-called Whitney form finite element approach, showing how electromagnetic fields around a cubic particle compare with FDTD results. Unfortunately space limitations do not allow us to describe other numerical methods, such as the dyadic Green's function method, that have also played a role in this field.

2. Analytical Models

A. Mie Theory. Mie theory in its standard presentation (a plane electromagnetic wave interacting with a spherical particle) is described in a number of textbooks,[21,23] so we will not go into the derivation here. The most common applications of Mie theory have been to the extinction spectra of nanoparticles, where only a single result from the theory is needed, namely, the formula for the extinction cross section:

$$C_{\text{ext}} = \frac{2\pi}{k^2}\sum_{\ell=1}^{\infty}(2\ell+1)\text{Re}(a_\ell + b_\ell) \tag{1}$$

where $k = 2\pi/\lambda$ and the coefficients a_ℓ and b_ℓ are given by (assuming that the magnetic permeabilities of the sphere and surrounding medium are the same):

$$a_\ell = \frac{m^2 j_\ell(x)[xj_\ell(x)]' - j_\ell(x)[mxj_\ell(mx)]'}{m^2 j_\ell(mx)[xh_\ell^{(1)}(x)]' - h_\ell^{(1)}(x)[mxj_\ell(mx)]'} \tag{2}$$

$$b_\ell = \frac{j_\ell(x)[xj_\ell(x)]' - j_\ell(x)[mxj_\ell(mx)]'}{j_\ell(mx)[xh_\ell^{(1)}(x)]' - h_\ell^{(1)}(x)[mxj_\ell(mx)]'} \tag{3}$$

In these expressions, "Re" denotes the real part of what follows, $x = ka$ with a being the sphere radius, $m^2 = \varepsilon_1/\varepsilon_0$, the functions $j_\ell(x)$ and $h_\ell^{(1)}(x)$ are, respectively, the spherical Bessel and Hankel functions, and ε_1 and ε_0 are the dielectric functions of the nanoparticle and surrounding medium, respectively. Computer codes for evaluating C_{ext} are widely available on the web, such as at the Nanosphere Optics Lab at nanohub.org.

Eqs 1−3 can easily be evaluated for particles that are 1000 nm or smaller. Figure 1a presents extinction efficiencies (the ratio of cross section to the geometrical area πa^2) for a silver sphere in vacuum and with sphere diameters of 10, 100, and 1000 nm. The dielectric function in these calculations is from Lynch and Hunter.[24] The 10 nm results show a typical dipole plasmon resonance at 360 nm, which red shifts and broadens considerably for the larger particle sizes. In addition, larger particles show higher multipole resonances to the blue of the dipole resonance. The red-shifting, broadening, and multipolar excitation that grows with increasing particle size is due to depolarization and radiative damping effects that arise from the finite size of the particle relative to the wavelength. Ultimately for large enough particles (1000 nm) this washes out plasmon resonance effects, leading to a structureless extinction spectrum in the visible.

For the 10 nm particle, the extinction cross section can be accurately represented using the quasistatic approximation, in which only the a_1 term in eq 1 is included, and the $k \to 0$ limit is taken in the evaluation. This leads to an extinction cross section of

$$C_{\text{ext}} = \frac{6\pi}{\lambda}(\varepsilon_0)^{1/2} V \,\text{Im}\, g \tag{4}$$

where

$$g = \frac{\varepsilon_1 - \varepsilon_0}{\varepsilon_1 + 2\varepsilon_0} \tag{5}$$

Here V is the particle volume, and "Im g" denotes the imaginary part of the function g. This expression shows that the dipole resonance occurs when the denominator of g is minimized, which means that the real part of ε_1 matches $-2\varepsilon_0$. This is satisfied at 360 nm for a small silver sphere, and the width of the plasmon resonance is determined by the imaginary part of ε_1 at that wavelength. For silver and gold, it is possible to represent ε_1 using the Drude model

$$\varepsilon_1(\omega) = 1 - \frac{{\omega_p}^2}{\omega(\omega + i\gamma)} + \chi^{ib}(\omega) \tag{6}$$

where ω is the angular frequency, ω_p is the bulk plasmon frequency, and γ is a width factor that determines the imaginary part of ε_1 provided that contributions from interband transitions contained in χ^{ib} can be ignored. Based on eqs 5 and 6, the plasmon frequency Ω is given by

$$\Omega = \frac{\omega_p}{\sqrt{1 + 2\varepsilon_0 + \mathrm{Re}\,\chi^{ib}}} \tag{7}$$

The width factor γ includes electron−phonon and other intrinsic electron relaxation mechanisms but not the radiative contributions to the width that were mentioned above because these are not included in the quasistatic approximation. In addition, for 10 nm particles, there are contributions to the width from scattering of the conduction electrons from the particle surfaces. These lead to an inverse dependence of width on particle size,[25] but it is of minor consequence here.

While the Mie theory application above is very common, an important but much less common application of Mie theory has been to study electromagnetic field enhancements in SERS. The theory was first developed in 1980 by Kerker, Wang, and Chew,[26] although others developed quasistatic and phenomenological models earlier as has been reviewed.[27−29] The Kerker theory considers a single molecule adsorbed onto a metal sphere with the molecule treated as a classical point dipole. The incident field interacts with the sphere to create an enhanced field at the molecule, which induces an oscillating dipole at the Stokes shifted frequency. Then the induced dipole emits waves, which scatter from the sphere to create an enhanced far-field SERS signal. The overall enhancement factor, G, thus involves two Mie theory applications: interaction of the sphere with the plane wave incident field, and interaction of the sphere with the dipole emitted field. The first application requires the electric fields from a standard Mie calculation, as are expressed in many places[23,26,30] using vector spherical harmonics. The second application can also be represented using vector spherical harmonics, as described by Kerker.[26]

If one defines the scattering plane (that associated with incident and scattered wavevectors) as the xz-plane and assumes that the exciting electric field is polarized perpendicular to this plane, then measurements of the components of the Raman scattered radiation whose polarization is also perpendicular to the plane result in what Kerker terms the Vv component of G, denoted G_{Vv}. A key result of the Kerker paper is that in the quasistatic limit, the SERS enhancement is given by

$$G_{Vv} = 5|1 + 2g|^2|1 + 2g_0|^2 = 5|1 + 2g + 2g_0 + 4gg_0|^2 \tag{8}$$

where g is given by eq 5 and g_0 is the same expression evaluated at the Stokes shifted frequency. Equation 8 expresses the enhancement in terms of a numerical constant "5" (which arises from orientation averaging effects) multiplied by the local field enhancement factors $|1 + 2g|^2$ and $|1 + 2g_0|^2$ at the incident and Stokes frequencies. This justifies the commonly used approximation that the SERS enhancement factor is the product of field enhancement factors at the incident and Stokes shifted wavelengths, but note that it only applies to specific molecular and field geometries in the quasistatic limit.

It is possible to use the complete multipole expansion for the vector fields to evaluate G_{Vv} exactly rather than using the quasistatic approximation. Figure 1b−d presents the results for 10, 100, and 1000 nm spheres, including comparison of the exact G_{Vv} with its quasistatic counterpart, as well as eq 7 with the additional approximation that the Stokes shift is neglected (giving the often cited $|E|^4$ enhancement). Figure 1b shows that the three expressions are similar for a 10 nm sphere. However for the 100 nm sphere, the exact expression is smaller below 400 nm but larger at long wavelengths. For the 1000 nm sphere, the exact expression is always a factor of at least 10 smaller, due to radiative damping contributions.

B. Quasistatic Theory for a Spheroidial. For a particle with size much smaller than the wavelength of the incident light, the quasistatic approximation can be applied to simplify the calculation of the absorption and scattering efficiency. In this limit, the extinction cross section of a metallic spheroid embedded in a homogeneous medium when the polarization of the incident light is parallel to the symmetry axis of the spheroid is given by eq 9 (which is a generalization of eqs 4 and 5):[3,20,23]

$$C_{ext} \propto \frac{1}{\lambda} \mathrm{Im}\left\{ \frac{\varepsilon_1 - \varepsilon_m}{\varepsilon_1 + \chi\varepsilon_m} \right\} \quad (9)$$

where ε_1 is the dielectric function of the metal, ε_m is the dielectric function of the surrounding medium, and χ is a shape factor for the particle that has the value 2 for a sphere, is <2 for an oblate spheroid, and is >2 for a prolate spheroid. A similar expression applies to the case where the polarization is perpendicular to the symmetry axis, except that now the χ parameter is <2 for a prolate spheroid and >2 for an oblate spheroid. This leads to two plasmon resonances, of which the red-most of these is of most interest in applications.

In many sensing applications based on localized surface plasmon resonance (LSPR) studies, one needs to calculate the extinction of nanoparticles coated with a layer of molecules. However, eq 9 considers a particle in a homogeneous environment. To treat an inhomogeneous environment consisting of a layer of molecules surrounded by a solvent, a primitive effective medium theory can be developed wherein the effective dielectric function of the surrounding medium is assumed to be of the form $\varepsilon_{m,effect} = \varepsilon_{mol} \cdot x + \varepsilon_m \cdot (1 - x)$ where ε_{mol} is the dielectric function of the molecule and x is a empirical parameter (between 0 and 1), which is determined by the relative amounts of molecules and solvent that are contained within the range of the electromagnetic field around the particle. Better effective medium theories include the Clausius−Mossotti, Maxwell−Garnett, and Bruggemann expressions,[23] but all lead to a linear dependence on x in the small coverage limit ($x < 0.05$), and this is where we will use this expression.

Equation 9 has recently been used to model the wavelength shift induced by resonant molecules in the extinction of Ag nanoparticles.[31] Here one evaluates this equation twice, once for ε_m referring to vacuum and once with ε_m referring to an effective medium composed of vacuum plus a thin layer of resonant molecules. Haes et al. studied the LSPR wavelength shift of Ag nanoparticles induced by a monolayer of resonant molecules [2,3,7,8,12,13,17,18-octakis(propyl)porphyrazinato] magnesium(II) (MgPz), which has an absorption maximum at 598 nm in ethanol solution.[10] In this work, the extinction wavelength shift induced by MgPz was calculated as a function of the plasmon resonance wavelength. The dielectric functions of MgPz were taken from Haes et al. and the parameter x in the effective medium theory was chosen as 0.01 to match the experimental data. (In principal, x should be determined from the fraction of the sensing volume that is occupied by the molecular layer; however this was not determined in these studies.) Figure 2a shows the extinction spectra of bare (solid lines) and MgPz-coated (dashed lines) Ag spheroids calculated using eq 9. Here the extinction wavelength of the Ag spheroid is varied by varying χ. Each pair of spectra with the same colors are calculated using the same χ. When the extinction maximum of the Ag spheroid is separated by more than 50 nm from the absorption peak of MgPz, the extinction maximum of the MgPz-coated Ag nanoparticle is red-shifted from that of the bare Ag nanoparticle. In addition, there is a small peak at ~600 nm in the spectrum due to absorption by MgPz. When the extinction wavelength of the Ag nanoparticle is close to the MgPz absorption peak, a dip in the extinction spectrum of the MgPz-coated Ag nanoparticle is found due to MgPz absorption. This phenomenon was not observed for dye molecules adsorbed on Ag nanoparticle arrays, probably because of particle inhomogeneity.[9,10] However, Lee and coworkers have recently demonstrated that when resonant molecules are adsorbed to a single Au nanoparticle and the resonant wavelength is close to a molecular resonance, a dip is produced in the extinction line shape.[32]

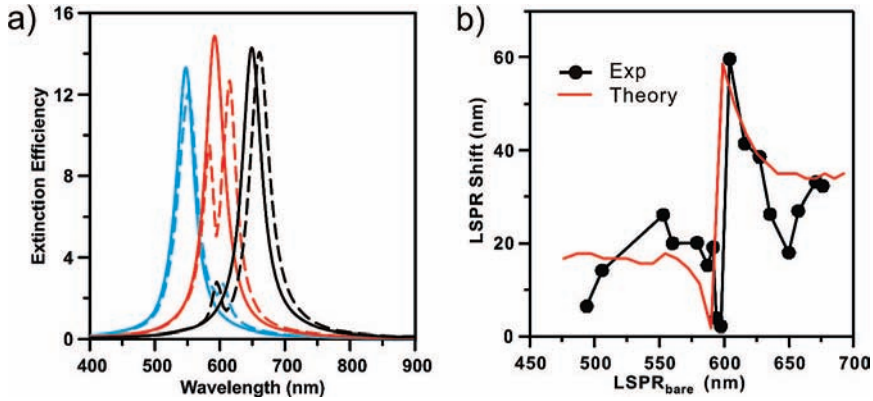

FIGURE 2. Extinction spectra of Ag spheroid/MgPz and LSPR shift induced by MgPz: (a) Extinction spectra of bare Ag spheroid (solid lines) and Ag spheroid with MgPz (dashed lines) with varying χ parameters. Each pair of spectra of the same color was calculated with the same χ. (b) LSPR shift of Ag nanoparticles induced by MgPz versus LSPR wavelength of bare Ag nanoparticles. The black line with dots is experimental LSPR shift data, and the red curve is the calculated LSPR shift.

Figure 2b shows the predicted LSPR wavelength shift (red solid line) in comparison with the experimental data (black solid line with dots). The figure shows that the modeling agrees well with the experiments, confirming that this method can be used to calculate the LSPR of metal nanoparticles coated with a resonant molecular layer.

3. Discrete Dipole Approximation

The DDA method was originally proposed by Purcell and Pennypacker[33] for describing light scattering from grains in the interstellar medium and then subsequently put on more quantitative footing for these applications by Draine, Goodman, and Flatau[34] through the DDSCAT program.[35] In the last 15 years, this method has been adapted to metal nanoparticle applications as has been reviewed.[18]

In the DDA method, the nanoparticles are represented as a cubic array of N polarizable elements whose polarizabilities α_i (i = 1, 2, ..., N) are determined from the nanoparticle dielectric function. The induced dipole P_i in each element in the presence of an applied plane wave field is $P_i = \alpha_i E_{\mathrm{loc},i}$ where the local field E_{loc} at r_i is the sum of the incident and retarded fields of the other $N - 1$ dipoles. For a given wavelength λ, this field is

$$E_{\mathrm{loc},i} = E_{\mathrm{inc},i} + E_{\mathrm{dipole},i} = E_0 \exp(ik \cdot r_i) - \sum_{\substack{j=1 \\ j \neq i}}^{N} A_{ij} \cdot P_j$$

$$\text{where} \quad i = 1, 2, \ldots, N \quad (10)$$

where E_0 and $k = 2\pi/\lambda$ are the amplitude and wave vector of the incident wave, respectively. The dipole interaction matrix **A** is

$$A_{ij} \cdot P_j = k^2 \, e^{ikr_{ij}} \frac{r_{ij} \times (r_{ij} \times P_j)}{r_{ij}^{\,3}} + e^{ikr_{ij}} (1 - ikr_{ij}) \frac{[r_{ij}^{\,2} P_j - 3r_{ij}(r_{ij} \cdot P_j)]}{r_{ij}^{\,5}}$$

$$(i = 1, 2, \ldots, N; \; j = 1, 2, \ldots, N; \; j \neq i) \quad (11)$$

where r_{ij} is the vector from dipole i to dipole j. Once the P_i's are determined by solving these equations, the extinction cross-section is determined from

$$C_{\mathrm{ext}} = \frac{4\pi k}{|\vec{E}^{\mathrm{inc}}|^2} \sum_{j=1}^{N} \mathrm{Im}[\vec{E}_j^{\,\mathrm{inc},*} \cdot \vec{P}_j] \quad (12)$$

A disadvantage of the DDA approach is that the coupling between dipoles is relatively long-ranged, so the interaction matrix is a full matrix. However Draine and co-workers have developed complex conjugate gradient methods to solve these problems, and the dipole interactions are evaluated using Fourier methods such that the computational effort for even 3D calculations is generally less than that for finite dif-

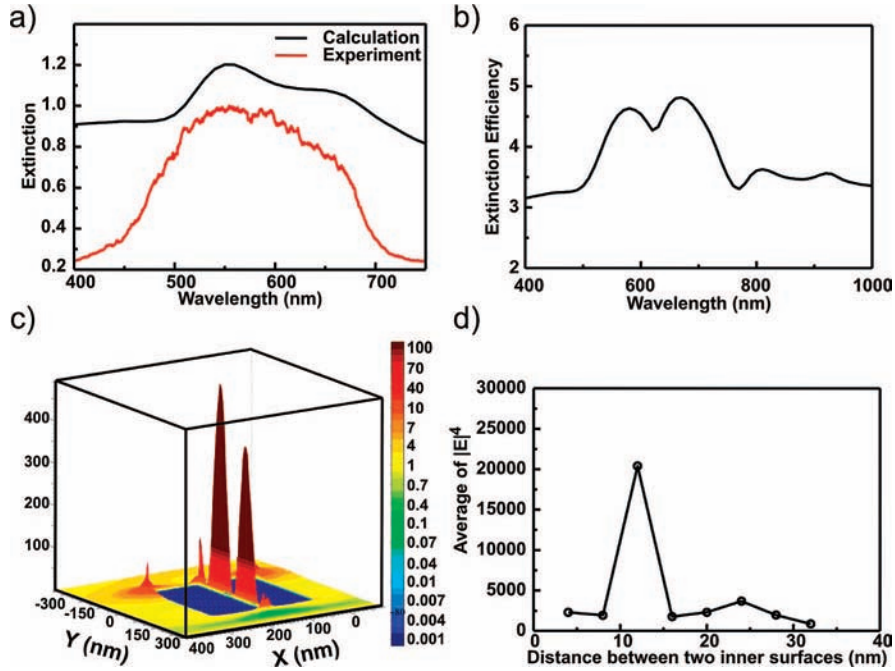

FIGURE 3. DDA results for a single gold disk and for a gold disk dimer: (a) the extinction spectrum of a gold disk from DDA compared with that from a dark field measurement; (b) the extinction spectrum of a gold disk dimer with a 12 nm separation; (c) contours of the local field $|E|^2$ for the $z = 0$ plane for the dimer with a 12 nm separation; (d) the average $|E|^4$ for an inner surface of the gold dimer versus distance between the two inner surfaces.

ferencing methods, at least for particles smaller than a few hundred nanometers in size. As a result, the DDA method has been widely used to describe the shape dependence of plasmon resonance spectra, including studies of triangular prisms,[36−38] disks,[39] cubes,[40] truncated tetrahedra,[41] shell-shaped particles,[42,43] small clusters of particles,[44] and many others.[18] Although DDA is not an exact method, comparisons of DDA results with other methods such as Mie theory indicate that errors in the extinction spectra are often less than 10%, with the overall multipole resonance mode structure being the same.

As an example of a DDA application, we consider the extinction and SERS enhancements associated with gold disks fabricated using on-wire lithography, expanding on an earlier study[39] in which DDA results were compared with experimental results. First consider a single gold disk with thickness 120 nm and diameter 360 nm. Assuming the wave vector is along the *x* axis and the symmetry axis is along *y* direction, the extinction spectrum from a DDA calculation is presented in Figure 3a, along with the results of experiments. This shows a major peak around 560 nm and a shoulder at 660 nm, which we have assigned to dipole excitation for *y* polarization and quadrupole excitation for *z* polarization, respectively. Both peaks are observed in the experimental measurements. The experiments also studied dimers of the same disk structure that are aligned along the symmetry axis and separated by a distance that can be varied from a few to many hundreds of nanometers. Figure 3b shows the extinction spectrum of the dimer for 12 nm separation. This shows the same two peaks but red-shifted to 590 and 690 nm, and we also see additional resonances at longer wavelength.

Also of interest in this work is the SERS enhancement factor associated with the gold dimer and particularly the dependence of this enhancement factor on the disk separation. Figure 3c shows contours of the enhancement factor $|E|^2$ for the dimer with 12 nm separation at a wavelength of 633 nm where primarily the longer wavelength *z* polarization resonance would be excited. The figure indicates that there is a hot spot between the disks for this resonance with fields that are enhanced by over 10^2 compared with the isolated disk for the same wavelength. This enhancement is strongly dependent on disk separation as is apparent from Figure 3d, with a separation of 12 nm giving an average $\langle|E|^4\rangle$ (averaged over one of the inner surfaces in the dimer) that is over 10^4. This strong dependence of peak enhancement on disk separation is similar to what is seen in the SERS experiments,[39] except that in the experiments the surfaces are rough so the separation giving peak enhancement is 30 nm rather than 12 nm. The overall enhancement factor in Figure 3d peaks at 2×10^5, which is not an especially high value for SERS measurements. However these studies are important because they demonstrate that peak enhancement is not associated with the smallest disk separation. This is because the dipole resonance shifts to the red as disk separation is decreased, leading to a detuning from the excitation wavelength for small separations.

4. FDTD and Related Finite Difference Methods

Finite difference methods solve Faraday's law and Ampere's law, eqs 13 and 14, in differential form over a grid-based domain (where field components are defined only at the grid points) using Taylor expansions for the derivatives.

$$\varepsilon \frac{\partial}{\partial t}\vec{E} = \nabla \times \vec{H} - \vec{J} \tag{13}$$

$$\mu \frac{\partial}{\partial t}\vec{H} = -\nabla \times \vec{E} \tag{14}$$

The most popular discretization is based on Yee's algorithm,[22,45] known as *the* FDTD method. In this method, $\vec{E}$ and $\vec{H}$ are shifted by half-grid points relative to each other, and central spatial and leapfrog time differences are used for the derivatives. A simple version of this can be generated for a 2D system in which the electric field only has *x* and *y* components, and the magnetic field has a *z* component. If the time step is denoted τ, then the following equations are used:

$$\begin{aligned} E_x^{n+1/2} &= E_x^{n-1/2} + \frac{\tau}{\varepsilon}\left[\frac{\partial H_z^n}{\partial y} - J_x^n\right] \\ E_y^{n+1/2} &= E_y^{n-1/2} + \frac{\tau}{\varepsilon}\left[-\frac{\partial H_z^n}{\partial x} - J_y^n\right] \\ H_z^{n+1} &= H_z^n - \frac{\tau}{\mu}\left[\frac{\partial E_y^{n+1/2}}{\partial x} - \frac{\partial E_x^{n+1/2}}{\partial y}\right] \end{aligned} \tag{15}$$

The finite difference methods described, although time-domain based, can be used to calculate the frequency domain spectra of nanoparticles using Fourier transforms.

FDTD methods have been extensively applied to studies of nanomaterial optical properties.[46] As an application of the 2D FDTD approach, we consider the transmission of light through a one-dimensional array of rectangular gold bars (actually wires). The length of each gold bar is fixed at 150 nm with a thickness of 8 nm. The spacing between the bars is varied between 5 and 300 nm to study the transition from film-like to particle-like behavior as the spacing is varied. In Figure 4, we present transmission probabilities versus wavelength of

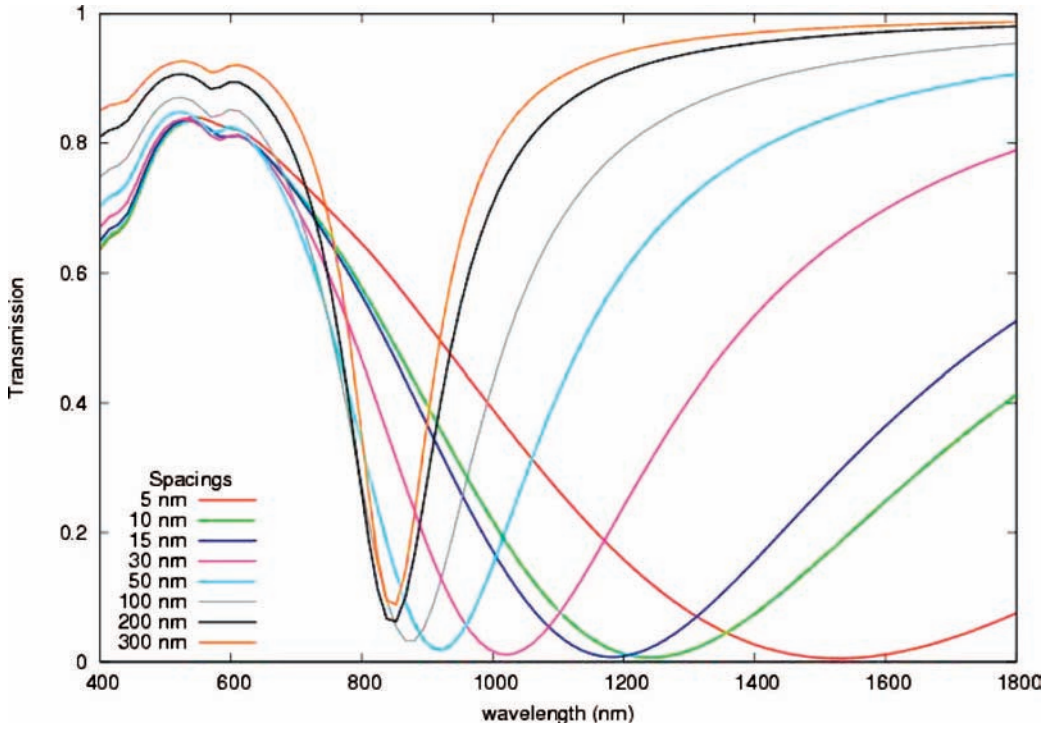

FIGURE 4. Transmission spectrum for a 1-D array of gold bars with various spacings between bars.

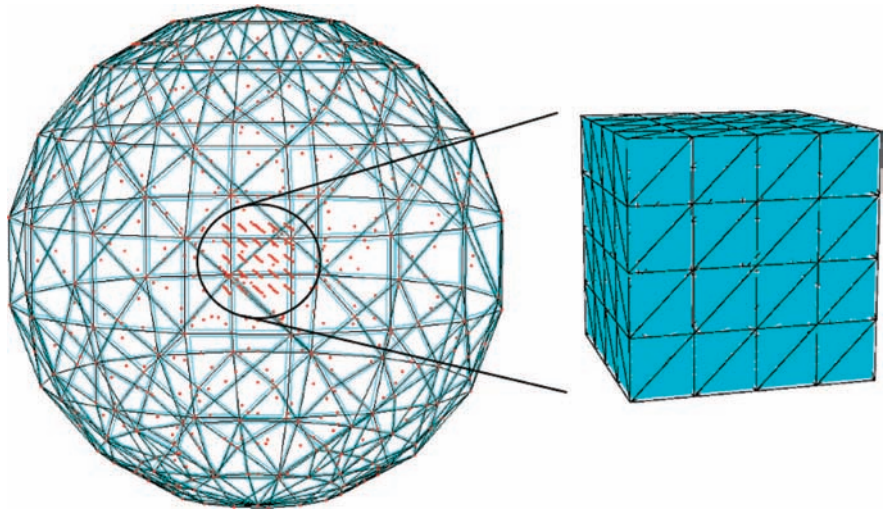

FIGURE 5. Finite element discretization suited to study a cubic nanoparticle. The full mesh is shown on the left, and the interior cubic region is shown on the right.

incident light. This shows a gradual evolution in results as spacing increases. Film-like behavior results in a maximum at 600 nm, corresponding to excitation of propagating surface plasmons, and a gradual drop-off of transmission at longer wavelengths (where the film becomes reflecting). Particle-like behavior leads to a minimum at 850 nm corresponding to plasmon excitation in each gold rod, with little coupling between rods. As the particles get closer together, we see a red-shifted plasmon resonance dip that moves from 850 to over 1500 nm. These results demonstrate how optical response can be switched using suitably chosen spacings. Note that the change in transmission possible in this problem is nearly 80%, a remarkable result given that the particles are only 8 nm thick.

The FDTD algorithm in three dimensions is considerably more demanding than the 2D calculations just presented. However, parallel implementations are relatively straightforward, and a number of applications have been presented in which simulation boxes over a micrometer in size have been considered.[47] Finite difference algorithms other than Yee's algorithm are also of interest. For example, in the Lax–Wendroff method,[48] $\vec{E}$ and $\vec{H}$ are updated concurrently,

rather than in a leapfrog fashion. One benefit of this scheme relative to the Yee algorithm is that one-sided differences, which are unstable in leapfrog schemes, can be used to truncate the domain.

Although powerful, finite difference methods are limited in their modeling capability due to their grid-based nature. Geometries must be approximated using a discrete grid, which results in what is known as the "staircasing" error. In addition, with normal Cartesian grids it is computationally expensive to model large domains while still resolving fine features (small grid spacings have to be used everywhere).

5. Finite Element Methods

A class of methods that do not suffer from the geometric modeling limitations of finite-difference methods, and is of particular interest for solving frequency-domain problems, are finite element methods (FEM).[49] When modeling metallic nanoparticles, FEM is typically used to solve the inhomogeneous vector wave equation,

$$\vec{\nabla} \times \left[\frac{1}{\mu_r}\vec{\nabla} \times \vec{E}\right] - k_0^2 \varepsilon_r \vec{E} = 0. \quad (16)$$

In FEM, the domain is divided into elements that are suited to the problem geometry and are often tetrahedral. Within each element $\vec{E}$ is approximated using a basis function expansion,

$$\vec{E} = \sum_{j=1}^{n} \vec{N}_j \phi_j \quad (17)$$

where the sum is over n interpolation points, $\vec{N}_j$ are chosen basis functions, and the ϕ_j are unknown coefficients. A solution to eq 16 is obtained by using the variational principle to determine ϕ_j. To obtain a meaningful solution, $\vec{N}_j$ is required to satisfy Gauss's law and appropriate boundary conditions on the surface of all elements. One such set of functions, based on the Whitney forms[50,51] and defined along the edges of elements, is

$$\vec{N}_j = l_j(\xi_{i1}\vec{\nabla}\xi_{i2} - \xi_{i2}\vec{\nabla}\xi_{i1}) \quad (18)$$

where l_j is length of edge j and the ξ_i are the simplex coordinates of node i (where nodes i_1 and i_2 are the end-points of edge j). Higher order basis functions can be constructed by multiplying eq 18 by Lagrange polynomials.[52]

FEM is ideal for modeling irregular geometries as well as efficiently simulating large domains containing fine details. The latter is accomplished by using small elements in regions where material properties change abruptly and fields are expected to significantly vary and large elements everywhere else. Because of this flexibility, problems that typically require multiple CPUs to solve by other methods can be solved using FEM on a single machine. To illustrate this, we simulated the scattering of 600-nm normal incident light (z-directed and y-polarized) by a 50-nm diameter cubic silver nanoparticle using both FEM and FDTD. For FDTD 1-nm grid spacings were used and the simulation was run for 200-fs to obtain accurate Fourier transformed fields. This took just over 8 h to complete using 256 2.6 GHz dual-core processors. For FEM, the domain was discretized using tetrahedral elements[53] and is shown in Figure 5. The basis functions in eq 17 multiplied by second-degree Lagrange polynomials were used, and the simulation took approximately 4 h to complete using a single 3.4 GHz processor. Calculated field profiles from both FDTD and FEM are shown in Figure 6. Even though the FEM results show slight artifacts, they agree well with FDTD, and this is tolerable considering the small amount of computing power required.

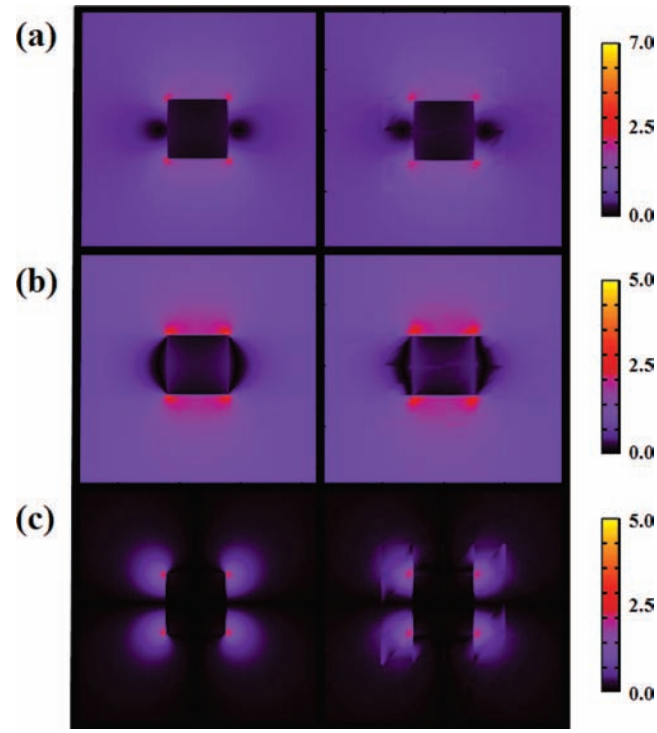

FIGURE 6. Field profiles of scattered light in the xy-plane by a cubic silver nanoparticle calculated with FDTD (left) and FEM (right): (a) $|\vec{E}|$; (b) $|E_y|$; (c) $|E_x|$.

6. Conclusion

The abundance of methods and applications that have been discussed here demonstrate the richness of this field and its impact on experiments. Moreover, what we have discussed is only a small sampling of the important work that has been done and that will be done in the future as more and more

sophisticated nanostructures are designed. Indeed, the emphasis in this Account has been on electromagnetics methods that have been used to describe isolated particles or small clusters, but much of the challenging work currently of interest involves more complicated nanostructures that combine metal and other particles, sometimes with thin films, to generate materials capable of plasmonic, photonic, or excitonic transitions. Fortunately the methods described in this Account give us powerful tools for treating these problems, sometimes by combining methods and sometimes by using advances in parallel computation to scale the codes so that very large (and complex) structures can be treated.

This research was supported by the NSF NSEC program under Grant EEC-0647560, the NSF MRSEC program under Grant DMR-0520513, Department of Energy Grant No. DEFG02-03-ER15487, DTRA JSTO Program (Grant FA9550-06-1-0558), DARPA, and the NSF Network for Computational Nanotechnology. We thank our many collaborators, including Stephen Gray, Richard Van Duyne, Chad Mirkin, Teri Odom, and Bartosz Grzybowski. Also we thank former members of the Schatz group, including Encai Hao, Traci Jensen, Lance Kelly, Anne Lazarides, Leif Sherry, Kevin Shuford, Wen-hui Yang, Linlin Zhao, and Shengli Zou.

BIOGRAPHICAL INFORMATION

Jing Zhao received a B.S. in chemical physics from University of Science and Technology of China in 2003. She is currently a Ph.D. candidate working with Prof. George C. Schatz and Richard P. Van Duyne at Northwestern University.

Anatoliy O. Pinchuk received his Ph.D. in Physics and Chemistry from the Institute of Surface Chemistry, National Academy of Science of Ukraine, in 1999. He held an appointment as a Docent at Kyiv Shevchenko University (2000−2002) and worked with Professor U. Kreibig, RWTH, Aachen, Germany, as a Humboldt Postdoctoral Research Fellow (2002−2004). Since 2004, he has been working with Professors George C. Schatz and B. A. Grzybowski at Northwestern University as a Postdoctoral Fellow.

Jeffrey M. McMahon received his B.S. degree from Western Washington University in 2005. He is currently a Ph.D. candidate at Northwestern University with Prof. George C. Schatz.

Shuzhou Li obtained his Ph.D. in Chemistry in 2006 at University of Wisconsin—Madison with Professor James L. Skinner. He is now a Postdoctoral Fellow with Professor George C. Schatz at Northwestern University.

Logan K. Ausman received his B.Sc. from the University of Wisconsin—Eau Claire in 2004. He is currently a Ph.D. candidate at Northwestern University with Prof. George C. Schatz.

Ariel L. Atkinson received a B.S. in chemistry from Binghamton University in 2005. His research focuses on the optical properties and interactions with metallic nanoparticles. He is currently a Ph.D. candidate at Northwestern University with George C. Schatz.

George C. Schatz is a Professor of Chemistry at Northwestern University. He received his B.S. in Chemistry from Clarkson University in 1971 and his Ph.D. in Chemistry in 1976 from Caltech.

FOOTNOTES

* Corresponding author. E-mail: schatz@chem.northwestern.edu. Telephone: (847) 491-5657. Fax: (847) 491-7713.

REFERENCES

1 Maier, S. A. Plasmonics: Metal Nanostructures for Subwavelength Photonic Devices. *IEEE J. Sel. Top. Quantum Electron.* **2006**, *12*, 1214–1220.

2 Willets, K. A.; Van Duyne, R. P. Localized Surface Plasmon Resonance Spectroscopy and Sensing. *Annu. Rev. Phys. Chem.* **2007**, *58*, 267–297.

3 Kreibig, U.; Vollmer, M. *Cluster Materials*; Springer-Verlag: Heidelberg, Germany, 1995; Vol. 25, p 532.

4 Schatz, G. C.; Van Duyne, R. P. Electromagnetic Mechanism of Surface-Enhanced Spectroscopy. In *Handbook of Vibrational Spectroscopy*; Chalmers, J. M., Griffiths, P. R., Eds.; Wiley: New York, 2002; Vol. 1, pp 759−774.

5 Zhao, J.; Zhang, X. Y.; Yonzon, C. R.; Haes, A. J.; Van Duyne, R. P. Localized Surface Plasmon Resonance Biosensors. *Nanomedicine* **2006**, *1*, 219–228.

6 McFarland, A. D.; Van Duyne, R. P. Single Silver Nanoparticles as Real-Time Optical Sensors with Zeptomole Sensitivity. *Nano Lett.* **2003**, *3*, 1057–1062.

7 Haes, A. J.; Van Duyne, R. P. A Nanoscale Optical Biosensor: Sensitivity and Selectivity of an Approach Based on the Localized Surface Plasmon Resonance Spectroscopy of Triangular Silver Nanoparticles. *J. Am. Chem. Soc.* **2002**, *124*, 10596–10604.

8 Haes, A. J.; Chang, L.; Klein, W. L.; Van Duyne, R. P. Detection of a Biomarker for Alzheimer's Disease from Synthetic and Clinical Samples Using a Nanoscale Optical Biosensor. *J. Am. Chem. Soc.* **2005**, *127*, 2264–2271.

9 Zhao, J.; Das, A.; Zhang, X. Y.; Schatz, G. C.; Sligar, S. G.; Van Duyne, R. P. Resonance Surface Plasmon Spectroscopy: Low Molecular Weight Substrate Binding to Cytochrome P450. *J. Am. Chem. Soc.* **2006**, *128*, 11004–11005.

10 Haes, A. J.; Zou, S.; Zhao, J.; Schatz, G. C.; Van Duyne, R. P. Localized Surface Plasmon Resonance Spectroscopy near Molecular Resonances. *J. Am. Chem. Soc.* **2006**, *128*, 10905–10914.

11 Elghanian, R.; Storhoff, J. J.; Mucic, R. C.; Letsinger, R. L.; Mirkin, C. A. Selective Colorimetric Detection of Polynucleotides Based on the Distance-Dependent Optical Properties of Gold Nanoparticles. *Science* **1997**, *277*, 1078–1080.

12 Haes, A. J.; Haynes, C. L.; McFarland, A. D.; Schatz, G. C.; Van Duyne, R. P.; Zou, S. Plasmonic Materials for Surface-Enhanced Sensing and Spectroscopy. *MRS Bull.* **2005**, *30*, 368–375.

13 Kelly, K. L.; Coronado, E.; Zhao, L. L.; Schatz, G. C. The Optical Properties of Metal Nanoparticles: The Influence of Size, Shape, and Dielectric Environment. *J. Phys. Chem. B* **2003**, *107*, 668–677.

14 Gonzalez, A. L.; Noguez, C. Optical Properties of Silver Nanoparticles. *Phys. Status Solidi C* **2007**, *4*, 4118–4126.

15 Noguez, C. Surface Plasmons on Metal Nanoparticles: The Influence of Shape and Physical Environment. *J. Phys. Chem. C* **2007**, *111*, 3806–3819.

16 Riikonene, S.; Romero, I.; Garcia de Abajo, F. J. Plasmon Tunability in Metallodielectric Metamaterials. *Phys. Rev. B* **2005**, *71*, 235104.

17 Gonzalez, A. L.; Noguez, C. Influence of Morphology on the Optical Properties of Metal Nanoparticles. *J. Theor. Comput. Nanosci.* **2007**, *4*, 231–238.

18 Zhao, L.; Zou, S.; Hao, E.; Schatz, G. C. Electrodynamics in Computational Chemistry. *Theor. Appl. Comput. Chem.* **2005**, 47–65.

19 Steele, J. M.; Grady, N. K.; Nordlander, P.; Halas, N. J. Plasmon Hybridization in Complex Nanostructures. *Springer Ser. Opt. Sci.* **2007**, *131*, 183–196.

20 Mie, G. Contributions to the Optics of Turbid Media, Especially Colloidal Metal Solutions. *Ann. Phys.* **1908**, *25*, 377–445.

21 Kerker, M. *The Scattering of Light and Other Electromagnetic Radiation*; Academic Press: New York, 1969.

22 Yee, K. S. Numerical Solution of Initial Boundary Value Problems Involving Maxwell's Equations in Isotropic Media. *IEEE Trans. Antennas Propag.* **1966**, *14*, 302–307.

23 Bohren, C. F.; Huffman, D. R. *Absorption and Scattering of Light by Small Particles*; Wiley-VCH: Weinheim, Germany, 2004.

24 Lynch, D. W.; Hunter, W. R. In *Handbook of Optical Constants of Solids*; Palik, E. D., Ed.; Academic Press: New York, 1985; pp 275−367.

25 Coronado, E. A.; Schatz, G. C. Surface Plasmon Broadening for Arbitrary Shape Nanoparticles: A Geometrical Probability Approach. *J. Chem. Phys.* **2003**, *119*, 3926–3934.

26 Kerker, M.; Wang, D.-S.; Chew, H. Surface Enhanced Raman Scattering (SERS) by Molecules Adsorbed at Spherical Particles. *Appl. Phys.* **1980**, *19*, E4159−4174.

27 Schatz, G. C. Theoretical Studies of Surface Enhanced Raman Scattering. *Acc. Chem. Res.* **1984**, *17*, 370–376.

28 Metiu, H.; Das, P. The Electromagnetic Theory of Surface Enhanced Spectroscopy. *Annu. Rev. Phys. Chem.* **1984**, *35*, 507–536.

29 Moskovits, M. Surface-Enhanced Spectroscopy. *Rev. Mod. Phys.* **1985**, *57*, 783–826.

30 Mackowski, D. W. Analysis of Radiative Scattering for Multiple Sphere Configurations. *Proc. R. Soc. London, Ser. A* **1991**, *433*, 599–614.

31 Zhao, J.; Jensen, L.; Sung, J.; Zou, S.; Schatz, G. C.; Van Duyne, R. P. Interaction of Plasmon and Molecular Resonances for Rhodamine 6g Adsorbed on Silver Nanoparticles. *J. Am. Chem. Soc.* **2007**, *129*, 7647–7656.

32 Liu, G. L.; Long, Y. T.; Choi, Y.; Kang, T.; Lee, L. P. Quantized Plasmon Quenching Dips Nanospectroscopy Via Plasmon Resonance Energy Transfer. *Nat. Methods* **2007**, *4*, 1015–1017.

33 Purcell, E. M.; Pennypacker, C. R. Scattering and Absorption of Light by Nonspherical Grains. *Astrophys. J.* **1973**, *186*, 705–714.

34 Goodman, J. J.; Draine, B. T.; Flatau, P. J. Application of the Fast Fourier Transformation Techniques to the Discrete Dipole Approximation. *Opt. Lett.* **1991**, *16*, 1198–1200.

35 Draine, B. T.; Flatau, P. J. User Guide to the Discrete Dipole Approximation Code Ddscat 6.1 http://Arxiv.Org/Abs/Astro-Ph/0409262v2. 2004.

36 Jin, R.; Cao, Y. C.; Hao, E.; Metraux, G. S.; Schatz, G. C.; Mirkin, C. A. Controlling Anisotropic Nanoparticle Growth through Plasmon Excitation. *Nature* **2003**, *425*, 487–490.

37 Shuford, K. L.; Ratner, M. A.; Schatz, G. C. Multipolar Excitation in Triangular Nanoprisms. *J. Chem. Phys.* **2005**, *123*, 114713.

38 Sherry, L. J.; Jin, R.; Mirkin, C. A.; Schatz, G. C.; Van Duyne, R. P. Localized Surface Plasmon Resonance Spectroscopy of Single Silver Triangular Nanoprisms. *Nano Lett.* **2006**, *6*, 2060–2065.

39 Qin, L.; Zou, S.; Xue, C.; Atkinson, A.; Schatz, G. C.; Mirkin, C. A. Designing, Fabricating, and Imaging Raman Hot Spots. *Proc. Natl. Acad. Sci U.S.A.* **2006**, *103*, 13300–13303.

40 Sherry, L. J.; Chang, S.-H.; Schatz, G. C.; Van Duyne, R. P.; Wiley, B. J.; Xia, Y. Localized Surface Plasmon Resonance Spectroscopy of Single Silver Nanocubes. *Nano Lett.* **2005**, *5*, 2034–2038.

41 Haes, A. J.; Zhao, J.; Zou, S.; Own, C. S.; Marks, L. D.; Schatz, G. C.; Van Duyne, R. P. Solution-Phase, Triangular Ag Nanotriangles Fabricated by Nanosphere Lithography. *J. Phys. Chem. B* **2005**, *109*, 11158–11162.

42 Hao, E.; Li, S.; Bailey, R. C.; Zou, S.; Schatz, G. C.; Hupp, J. T. Optical Properties of Metal Nanoshells. *J. Phys. Chem. B* **2004**, *108*, 1224–1229.

43 Henzie, J.; Shuford, K. L.; Kwak, E.-S.; Schatz, G. C.; Odom, T. W. Manipulating the Optical Properties of Pyramidal Nanoparticle Arrays. *J. Phys. Chem. B* **2006**, *110*, 14028–14031.

44 Hao, E.; Schatz, G. C. Electromagnetic Fields around Silver Nanoparticles and Dimers. *J. Chem. Phys.* **2004**, *120*, 357–366.

45 Hagness, S.; Taflove, A. *Computational Electrodynamics: The Finite-Difference Time-Domain Method*, 3rd ed.; Artech: Boston, 2005.

46 Teixeira, F. L. Fdtd/Fetd Methods: A Review on Some Recent Advances and Selected Applications. *J. Microwaves Optoelectron.* **2007**, *6*, 83–95.

47 McMahon, J. M.; Henzie, J.; Odom, T. W.; Schatz, G. C.; Gray, S. K. Tailoring the Sensing Capabilities of Nanohole Arrays in Gold Films with Rayleigh Anomaly-Surface Plasmon Polaritons. *Opt. Express* **2007**, *15*, 18119–18129.

48 Lax, P. D.; Wendroff, B. Systems of Conservation Laws. *Comments Pure Appl. Math* **1960**, *13*, 217–237.

49 Jin, J. *The Finite Element Method in Electromagnetics*, 2nd ed.; Wiley: New York, 2002.

50 Whitney, H. *Geometric Integration Theory*; Princeton University Press: Princeton, NJ, 1957.

51 Nedelec, J. C. Mixed Finite Elements in R3. *Numer. Methods* **1980**, *35*, 315–341.

52 Graglia, R. D.; Wilton, D. R.; Peterson, A. F. Higher Order Interpolatory Vector Bases for Computational Electromagnetics. *IEEE Trans. Antennas Propag.* **1997**, *AP-45*, 329–342.

53 Tetgen: A Quality Tetrahedral Mesh Generator. http://tetgen.berlios.de (accessed April 13, 2008).